Record grounded glacier retreat caused by an ice plain calving process in Antarctica

Naomi Ochwat[1,2]*, Ted Scambos[1], Robert S. Anderson[2,3], J. Paul Winberry[4], Adrian Luckman[5], Etienne Berthier[6], Maud Bernat[6], Yulia K. Antropova[7]

[1]Earth Science Observation Center, Cooperative Institute for Research in Environmental Science, University of Colorado Boulder, Boulder, CO, USA
[2]Department of Geological Sciences, University of Colorado Boulder, Boulder, CO, USA
[3]Institute for Arctic and Alpine Research, University of Colorado Boulder, Boulder, CO, USA
[4]Department of Geological Sciences, Central Washington University, Ellensburg, WA, USA
[5]Department of Geography, Faculty of Science and Engineering, Swansea University, UK
[6]Université de Toulouse, LEGOS (CNES/CNRS/IRD/UT3), Toulouse, France
[7]Department of Geography and Environmental Studies, Carleton University, Ottawa, ON, Canada

*Corresponding author: naomi.ochwat@colorado.edu

Abstract

Understanding and predicting glacier instabilities represents one of the greatest challenges in forecasting future sea level rise. Here, we present a study of Hektoria Glacier on the Eastern Antarctic Peninsula, which underwent an unprecedented rate of glacier retreat of ~25 km from January 2022 to March 2023, with an exceptional retreat period in November-December of 2022. Glacier retreat commenced immediately following the loss of decade-old fast ice in the Larsen B embayment. The retreat coincided with an almost 6-fold increase in flow speed and 40-fold increase in glacier thinning, compared to the period prior to the loss of the fast ice in 2022. The November-December accelerated retreat began with a transition from tabular iceberg calving to buoyancy-driven calving of a lightly grounded ice plain area. In this two-month period, the glacier retreated a total of 8.2 ± 0.2 km, a retreat rate nearly an order of magnitude faster than any published value. The Hektoria case implies that glaciers with ice plain bed geometry can be easily destabilized. The resulting extreme effect on ice discharge underscores the importance of identifying outlet glacier regions with similar characteristics.

MAIN TEXT

Introduction

Glaciers that feed ice shelves or landfast ice areas (hereafter, ‘fast ice’) are subject to dynamical changes upon the removal of these stabilizing features[1,2]. As the climate continues to warm, ice shelves and multi-year fast ice are increasingly susceptible to collapse[3], thus exposing the glaciers to new stress regimes and external forcings. These dynamical changes have been documented in detail on the Antarctic Peninsula (AP) following the loss of the Prince Gustav Ice Shelf[4], Larsen A[5,6] and Larsen B ice shelves[7,8], the Wilkins Ice Shelf[9], and others. These areas provide a natural observatory to examine potential feedbacks and instabilities that may occur in other, larger glacier systems that include at-risk floating ice.

In particular, the Larsen B Ice Shelf and tributary glaciers were relatively stable until the mid-1990s. In early 2002 the ice shelf disintegrated over several weeks, initiating a substantial mass flux change in the glaciers that fed it[10,11]. The glaciers rapidly retreated into their fjords, thinned, and accelerated up to 8 times their pre-shelf-retreat speeds[10]. In 2011, the embayment filled with fast ice, partially stabilizing the glaciers, allowing them to advance into the embayment, thicken, and slow, forming extensive ice tongues[1, 12]. In 2022, the decade-old fast ice broke out, causing the glaciers to lose their 300+ meter thick floating ice tongues and rapidly retreat[1,13]. Ochwat et al.[1] document the triggers that caused the fast ice to break out and the subsequent glacier acceleration and thinning through spring 2023. They found that Crane, Hektoria, Green, and Jorum Glaciers accelerated up to 2-fold during the first 13 months following the January 2022 break-out. Fluegel and Walker[14] document the 20-year record of the Hektoria-Green (hereafter, HG) glacier system, and suggest the recent retreat was exacerbated by atmospheric and oceanic conditions. However, these studies do not propose a clear cause for Hektoria Glacier's extraordinary retreat in 2022-2023.

There are several processes that can lead to marine-terminating glacier destabilization. The Marine Ice Cliff Instability (MICI) theory describes a process whereby high (>100 m) unsupported marine-terminating ice cliffs result in very high ice-front stresses that drive rapid ice-front calving; however, it has yet to be observed in nature[15-17]. The Marine Ice Sheet Instability (MISI) posits that outlet glaciers retreating into retrograde slopes will experience an accelerating grounding line retreat, creating thick floating or near-floating ice at their ice fronts. The increased ice thickness drives rapid ice flow, resulting in thinning, further retreat, and ultimately ice sheet collapse[18-20]. A potential variation of MISI occurs when there is an ice plain, which is a flat region of bedrock upstream of the grounding line, where the glacier ice has a very low slope (< 5°), is near hydrostatic equilibrium[21,22], and is lightly grounded or ephemerally grounded with the tidal cycle[21]. The presence of an ice plain can promote a rapid grounding line retreat and buoyancy-driven, rotational calving that results from the lifting force of the sub-sea-level ice in the calving block when the calved segment is narrow relative to its height. This process has been discussed previously, in models[15,23,24] and in observations[17,23,25,26]. Observations of paleo-deglaciation have suggested grounding line retreat rates of hundreds of meters per day[27]. Here we infer that this process led to extremely high rates of glacier retreat and calving as the entire ice plain went afloat almost instantaneously[27].

In this study, we detail the rapid terminus retreat of Hektoria Glacier, one of the glaciers in the HG system, over an extensive ice plain in the downstream glacier region. While this ice plain could be inferred from previous studies of Hektoria Glacier[1,28], we review and add to the evidence for it and propose a retreat mechanism based on buoyancy-driven calving across its extent. We document the retreat phases during the 2022-2023 accelerated retreat period, including an evaluation of changes in calving style and characteristics of the glacier terminus and icebergs. We include key information from glacio-seismic data that support our ice plain and buoyancy-driven calving model for the 2022-2023 retreat, and discuss the potential significance of this process for the Antarctic ice sheet.

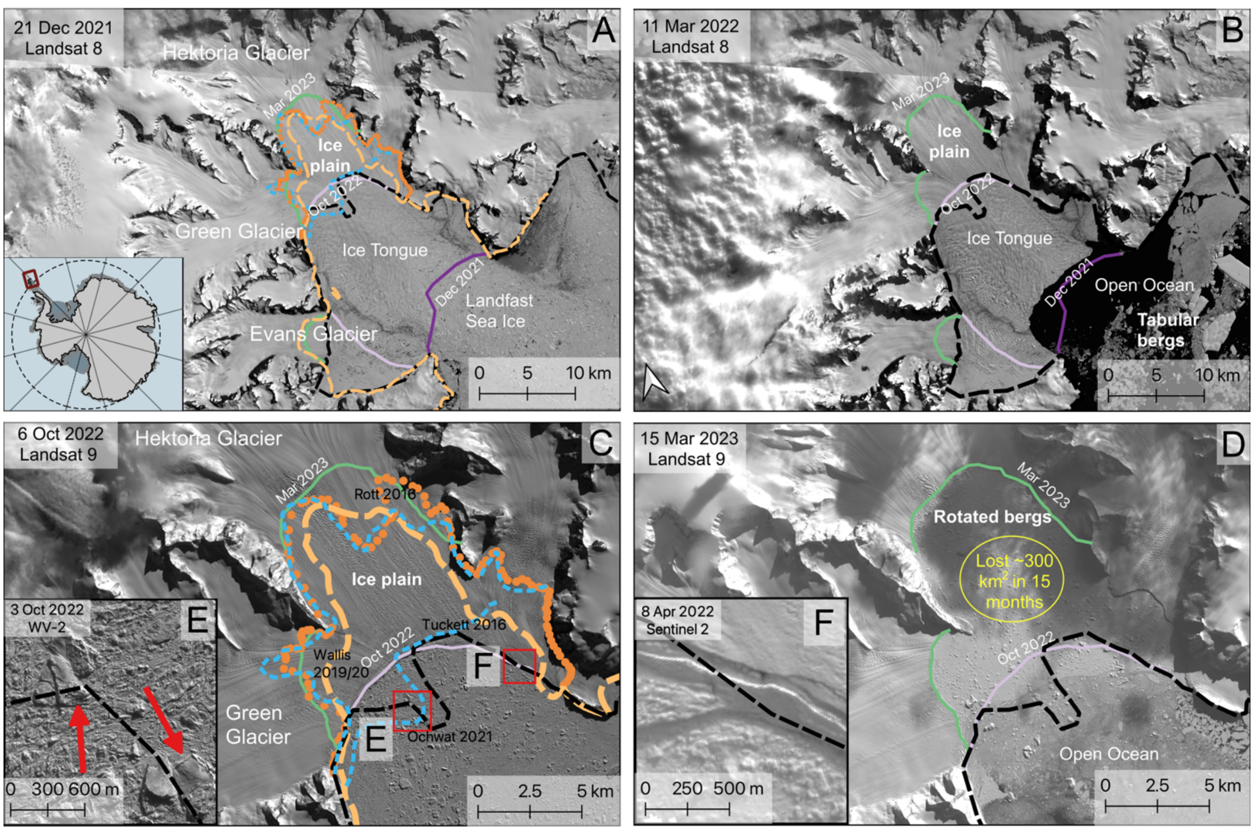

Fig. 1: The 2022-2023 accelerated retreat of Hektoria and Green glaciers. A) Hektoria and Green glaciers prior to the loss of decade-old fast ice in the Larsen B embayment. Grounding lines for this pre-fast-ice-loss period from previous studies are shown as dark orange[33], light orange[34], and light blue[29] dashed lines, and our preferred initial grounding line as a black[1] dashed

line. The area of the ice tongue lies between the dark purple December 2021 ice front line and this black dashed line, and the inferred ice plain lies between the black dashed line and the green March 2023 glacier terminus from this study. B) March 2022 image just after the fast ice break-up at the onset of ice tongue retreat through tabular calving. C) Landsat image showing HG at the beginning of the period of accelerated calving, with the light purple line indicating the ice front at this time; D) Image of the mélange area of the collapsed ice plain and the more stable terminus location of Hektoria in March 2023 (green line). E) Toppled icebergs (red arrows) in October 2022 image as calving continues across the lower grounding lines after ice tongue loss; F) April 2022 image showing forwardly-rotated iceberg at the transition from floating ice tongue to grounded ice plain.

Phases of the 2022-2023 retreat

After the loss of the Larsen B embayment fast ice, the HG system can be characterized by four distinct phases of terminus behavior, two phases of retreat (phase 1 and 3) and two phases of stability (phase 2 and 4), identified by iceberg morphology and calving style (Fig. 1; Fig. 2; Supplemental Video 1). Phase 1 of the retreat occurred immediately after the fast ice break-up in February-March 2022, when the 300+ m thick floating ice tongue disaggregated in a series of small tabular calvings[1] (Fig. 2B). During this period HG lost 16 km of floating ice (~216 km^2) at a rate of up to 0.8 km/day. Tabular bergs are identified by their aspect ratio and a dark rough upper surface that resembles the glacier surface[25,29,30].

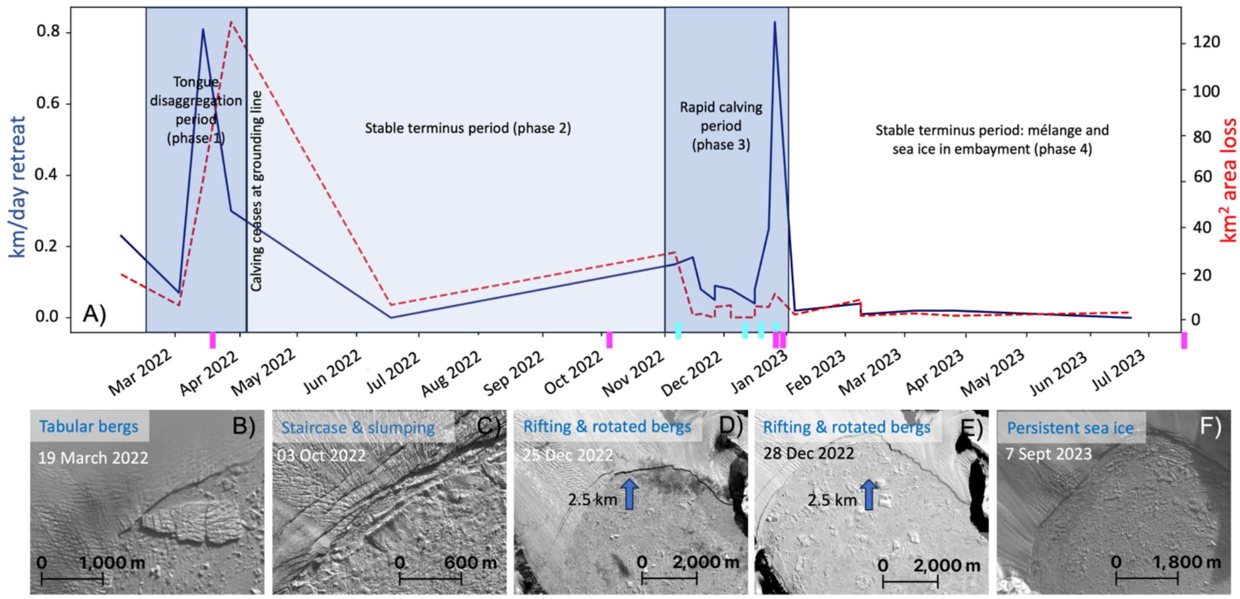

Fig. 2. A: Hektoria Glacier retreat rate and ice area loss from February 2022 to August 2023. Cyan ticks mark the occurrence of glacier earthquakes detected on 6 November 2022, 12, 19, and 25 December 2022; seismograms are shown in Fig. 5 and Extended Data Fig. 5. Magenta ticks indicate the acquisition date of the image panels in B-F, illustrating the changes in glacier front and iceberg morphologies during the key periods of retreat. Satellite images in B-F are from Maxar Worldview (C and D), PlanetScope (E; Image © 2022 Planet Labs PBC), and Landsat 9 (B and F). Panels D & E show the same areal extent.

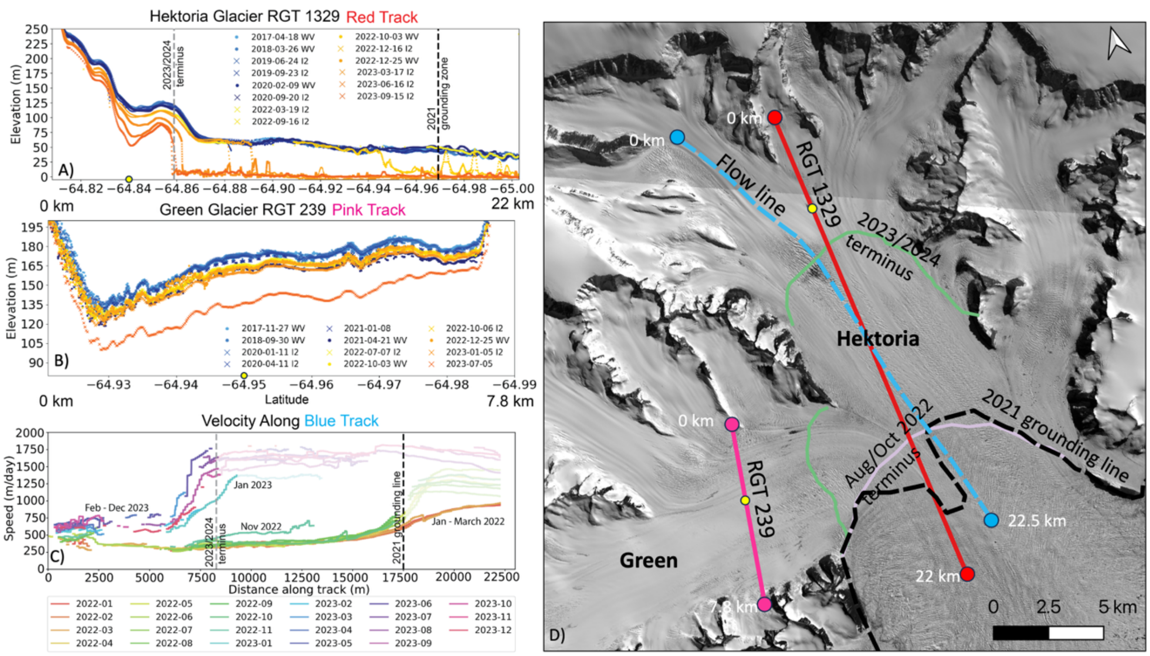

Fig. 3: Time series of elevation and velocity of Hektoria and Green Glaciers. A) Elevation profile along Hektoria Glacier (red track; Reference Ground Track (RGT) 1329) from April 2017 to September 2023. B) Elevation profile across Green Glacier (pink track; RGT 239) from November 2017 to July 2023. C) Velocity along Hektoria Glacier's central flow line (blue track). The profiles are opaque for glacier ice and become transparent at the transition to iceberg mélange. D) 21 December 2021 Landsat 8 image with the ICESat-2 tracks and along flow track, yellow dots are elevation thinning measurement locations.

A period of terminus stability (phase 2) ensued during the 2022 austral winter (June-Aug), when sea ice and mélange remained in the immediate vicinity of the glaciers' fronts (Fig. 2), likely providing backstress and ocean swell dampening that temporarily suppressed further calving[31]. During phase 2, Hektoria Glacier accelerated by over 70% and began to thin dynamically (Fig. 3A and C); the same occurred on Green Glacier (Fig. 3B, Extended Data Fig. 4). Prior to the fast ice break-out (2017 – 2021), the HG system thinned at an average rate of 2-3 m/yr (Fig. 3A and B). Following the fast ice break-out (March - December 2022), the thinning rate increased to 19 ± 2 m/yr for Hektoria and 4 ± 2 m/yr for Green Glacier.

By October 2022, tabular-style calving ceased and Hektoria Glacier's ice front developed a staircase-like structure, listric faulting and slumping, with the unfractured glacier front height ~50 m above sea level (Fig. 2C, Extended Data Fig. 3). We infer that listric slumping leads to buoyancy-driven calving through increased upward force on the lower (submerged) slump block, lifting and fracturing the upper ice and calving a toppled iceberg in a "bottom-out" style[26] (Fig. 2C, Extended Data Fig. 3).

As Hektoria entered phase 3, buoyancy-driven calving dominated, producing toppled icebergs that have a relatively smooth upper surface with a scalloped texture consistent with an exposed fracture face, and blue appearance in multi-spectral satellite images due to exposed interior ice. In many cases, the original glacier upper surface can be identified by its relatively flat profile in the toppled icebergs. An analysis of toppled iceberg dimensions suggests that the minimum ice thickness of this downstream edge of the ice plain is at least 407 ± 11 m and thickens to 492 ± 30 m as it retreats (Extended Data Figs. 1 and 4).

During the period of accelerated retreat (phase 3; November-December 2022), calving occurred at unprecedented rates for grounded ice, reaching 0.8 km/day, resulting in the loss of an additional 8.2 ± 0.2 km of glacier front and 40 km^2 of total glacier area. This calving coincided with glacier earthquakes that were captured by the multi-national seismic sensor networks in the region (blue ticks in Fig. 2). A notably rapid period of grounded ice retreat occurred 25-28

December when 2 ± 0.01 km retreated, covering 11.2 ± 0.01 km^2 (Fig. 2D and E). From January to March 2023 Hektoria retreated a further 1.5 ± 0.03 km, losing 13 ± 0.04 km^2. Phase 3 and 4 together (November 2022-March 2023) resulted in a total loss of 84 ± 0.5 km^2 of grounded ice with a minimum volume loss of 36 ±1 km^3. From December 2022 to March 2023 the thinning rate for the remaining portion of Hektoria Glacier increased to 64 ± 2 m/yr (Fig. 3A). By September 2023, thinning rates at Hektoria and Green reached 80 ± 2 m/yr and 54 ± 2 m/yr, respectively (yellow dots in Fig. 3).

Phase 4 is characterized by a period of relative terminus stability that began in March 2023 and persists as of December 2024. Hektoria has had a near-fixed terminus location, yet its dynamics continue to change substantially as it calves, accelerates, and thins (Fig. 3). The terminus is no longer fronted by a cliff, and it continues to slump into a mélange that fills the HG embayment (Supplemental Video 2).

Assessment of ice plain conditions in Hektoria Glacier

Several recent studies have presented grounding lines of Hektoria Glacier that show substantial disagreement (Fig. 1). These discrepancies likely result from different methods used. Tuckett et al.[29] identified grounded ice surface features and identified breaks-in-slope, one near the grounding line locations suggested by Rott et al.[32] and Wallis et al.[33], and one near our identified grounding line[1]. The two breaks-in-slope can identify an ice plain[21,22]. This suggests that Rott et al.[32], via the break-in-slope method, identified Point C, the coupling point, typical of the upstream limit of an ice plain[21,22]. Point C is not the true grounding line in an ice plain system. The Wallis et al.[33] grounding line was determined by identifying cyclical variations in the radar range (after subtracting displacement due to ice velocity) in Sentinel-1 synthetic aperture radar. However, the range variations can be interpreted in two ways: as vertical motion due to tides, or as cyclical tidally-paced variations in flow speed. Wallis et al.[33] interpret the range variations as vertical motion. We suggest that at lower tide levels the terminus of the glacier is more grounded, causing a rise in basal shear stress that induces a slowdown[34,35].

In the downstream Hektoria Glacier trunk, Ochwat et al.[1] noted that surface undulations (10s of meters relief, few km spatial scale) appear to be fixed in place in the period 2011-2022 (Fig. 4A-D), leading to their assessment that the region downstream of the Rott et al.[32] and Wallis et al.[33] grounding lines was in fact lightly grounded. Downstream of Ochwat et al.[1] grounding line position, long-wavelength undulations advect with the speed of the glacier. They interpreted these as the surface expression of bottom crevasses (flexion zone) beneath an ice tongue, indicating floating ice.

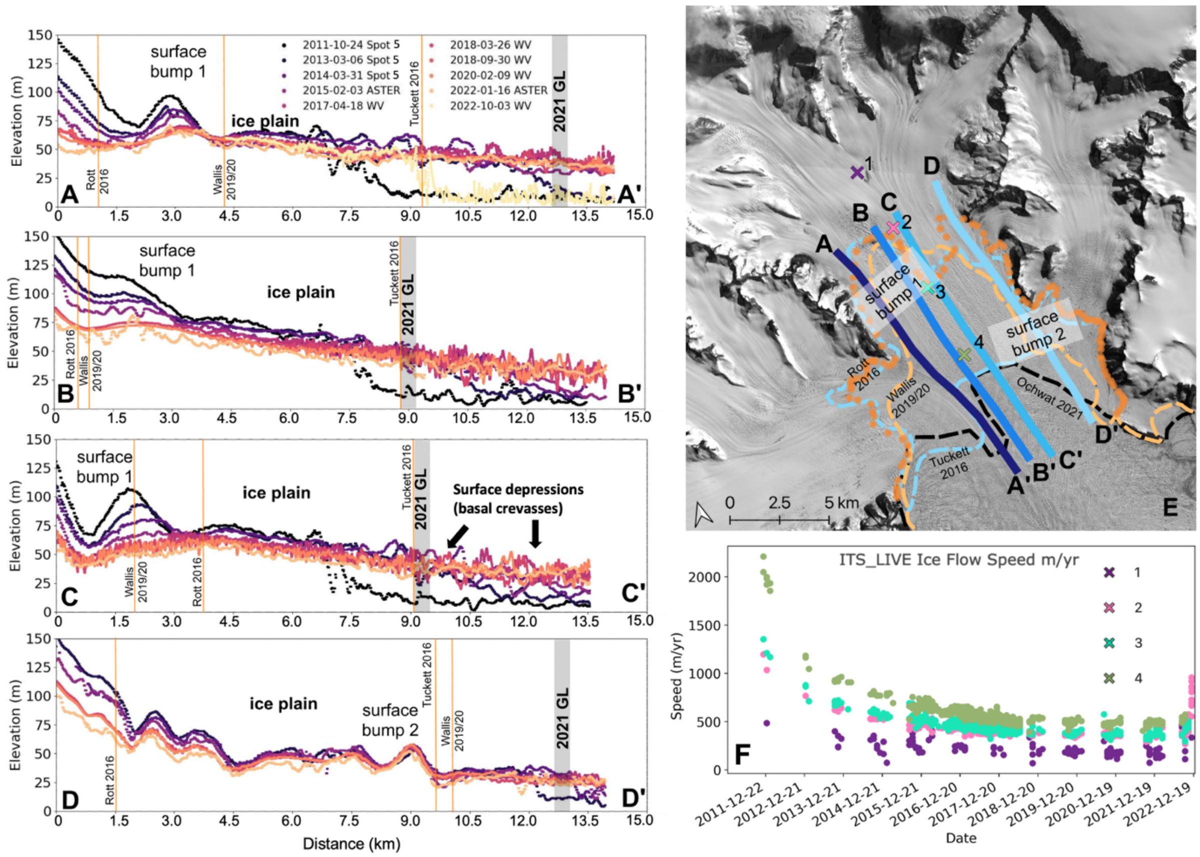

Fig. 4: Time series of elevations along four profiles in the Hektoria-Green glacier system and corresponding velocities. Panels A-D) four elevation profiles of satellite stereo-image derived DEMs spanning 2011 to late 2022, with several surface features and interpreted state of the glacier ice labeled, including “surface bump 1” and “surface bump 2”, which were not advected downstream. Black arrows highlight the moving position of surface features interpreted as bottom crevasses. Panel E) Landsat 8 image from 21 December 2021 showing elevation profile locations, recent published grounding line locations, the date of the data used to infer their location, including Ochwat 2021 (black dashed line[1]), Wallis 2019/20 (light orange dashed line[33]), Tuckett 2016 (blue dashed line[28]), and Rott 2016 (dark orange points[32]). Panel F shows ITS_LIVE velocity data[55] from 2011-2022 at four points on Hektoria’s central flow line, marked by the colored “x”s.

In our study, all profiles show two distinct breaks in the slope; upstream of the “bump 1” feature (Fig. 4A-D), and just downstream of the “bump 2” feature, below which the inferred bottom crevasses appear. The two distinct breaks in the slope support our interpretation of an ice plain area of the glacier[22,28,36] (Fig. 6).

As retreat proceeded past the Tuckett-Ochwat grounding lines, the ice front exhibited a ‘staircase’ listric fracture and calving style implying a substantial change in stresses and a non-zero basal shear stress there, hence a transition from floating to grounded ice plain[26]. IceBridge radar data from 2017 show reflection strength changes that indicate a transition from grounded to floating ice around the Tuckett-Ochwat grounding line (Extended Data Fig. 2). IceBridge radar profiles from other years in the region were inconclusive.

The seismic events identified in the multi-national seismic sensor networks confirm the grounded nature of the ice front during phase 3 (Fig. 2 and 5). We identified no events in the Hektoria region prior to November 2022, followed by a series of glacier earthquakes (GEQs) that occurred simultaneously with large glacier retreat events on the ice plain in satellite image time-series (Fig 1, Fig. 5, Extended Data Fig. 5). Modeling the observed seismic waveforms indicated they were generated by a nearly horizontal source oriented roughly perpendicular to the Hektoria calving front with peak forces of ~0.5-2 x 10^{10} N, consistent with generation by calved icebergs with mass of ~10^{11} kg (ref.[37,38], Fig. 5; Extended Data Figs. 7). Buoyancy-driven calving can produce glacier earthquakes when icebergs capsize at the terminus of the glacier, creating a force against the ice front and the glacier bed; this momentarily creates a cm-scale speed reversal in the glacier and an upward force on the Earth[26,39,40]. These types of earthquakes are characterized by long periods (30-150 s, moment-magnitude Mw = 5 tectonic earthquake) and are detectable globally[37]. Six GEQs occurred at Hektoria Glacier during the rapid retreat, four of which correspond closely to observed retreat events at Hektoria's ice front (Fig. 5; Extended Data Fig. 5).

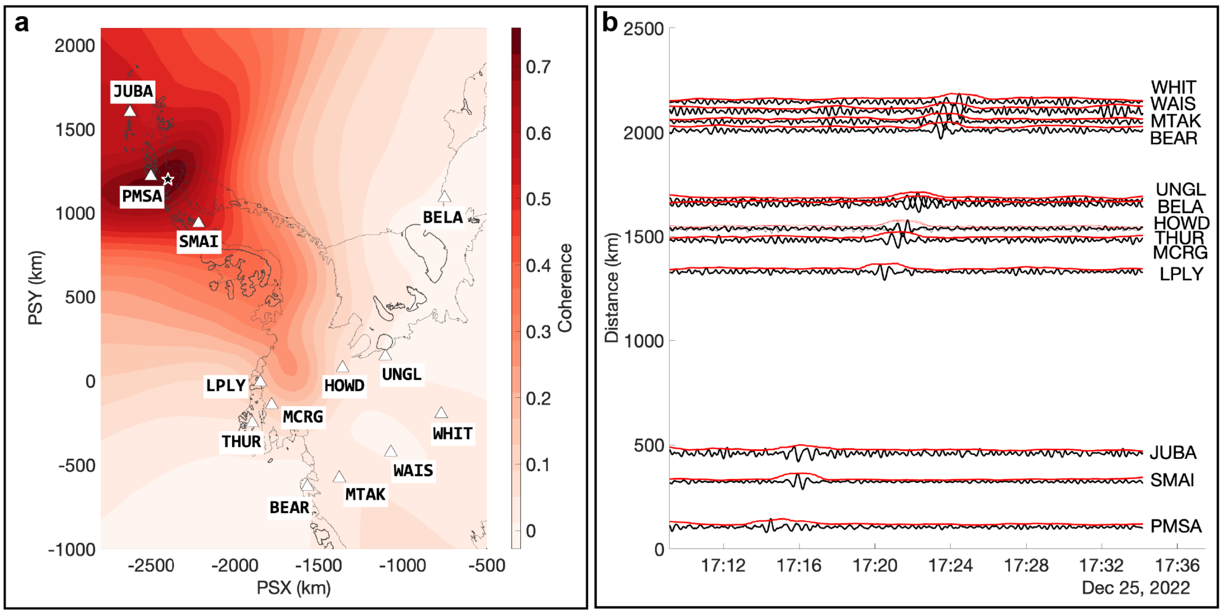

Fig. 5. The glacial earthquake of 25 December 2022: location and waveforms. A) Our location estimate for this event. Higher coherence indicates more likely source location with star denoting best fitting location. White triangles are the locations of seismic stations used in the location estimation. B) Vertical seismic waveforms (black) and their envelopes (red) after a 20-50 s bandpass filter is applied. Trace amplitudes are normalized and sorted by distance to source location.

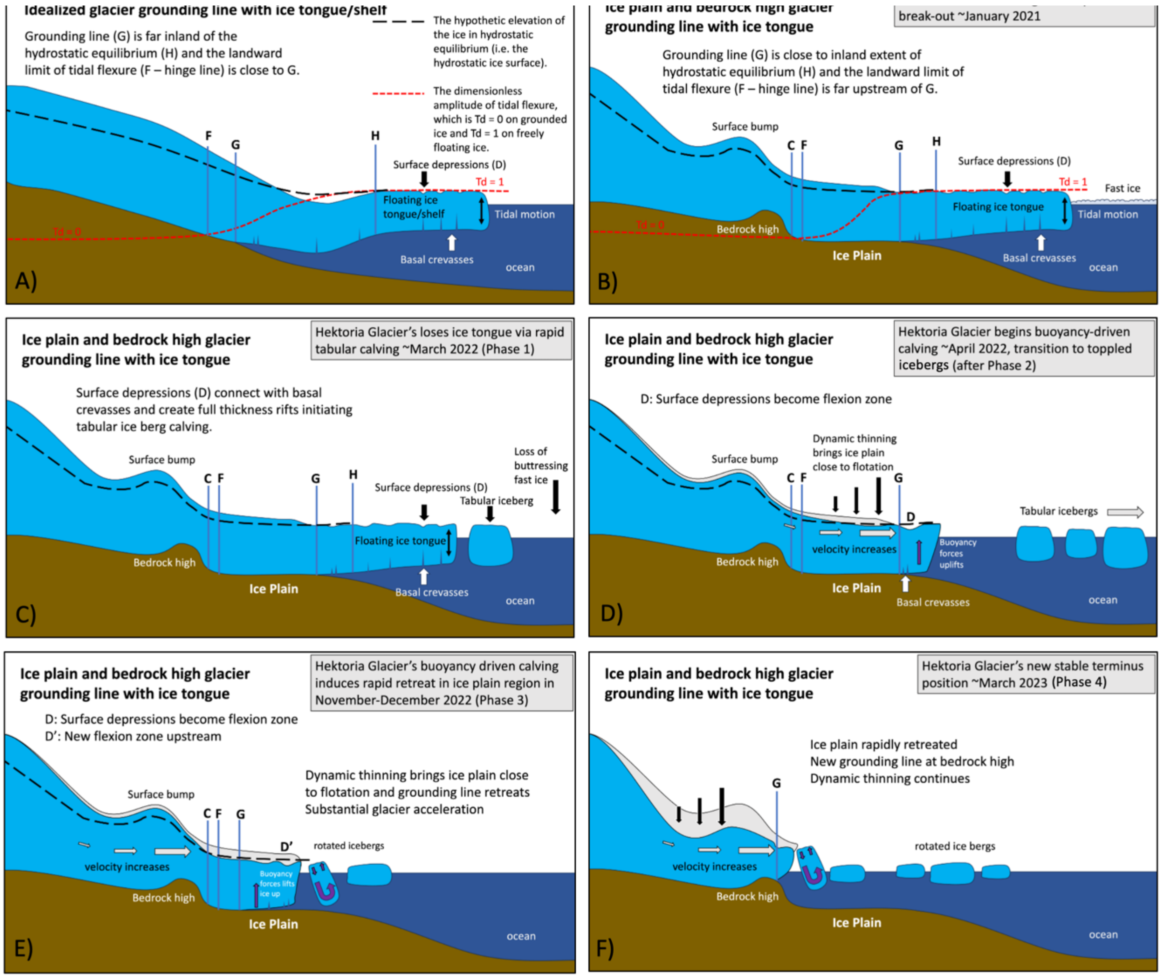

Fig. 6: Time series schematic of an idealized glacier cross section and Hektoria Glacier's configuration and rapid retreat. Black dashed line is the elevation of an ice surface with the ice in hydrostatic equilibrium; the red dashed line is a dimensionless amplitude of tidal flexure where Td = 0 on grounded ice and Td = 1 for ice in full hydrostatic equilibrium. Point C is the coupling line, the most notable break in the slope of an ice plain; Point F is the landward limit of tidal flexure (hinge line); Point G is the grounding line, the last point at which the glacier touches the bedrock surface and may migrate with tides; Point H is the landward limit of hydrostatic equilibrium of floating ice shelf or tongue. A) Idealized glacier and ice-shelf configuration; B) A conceptual sketch of Hektoria Glacier's profile prior to the fast ice break-out, showing a bedrock high similar to that inferred in Fig. 3 (adapted from Friedl et al.[22] and Batchelor et al.[27]); C)

Hektoria Glacier system as it loses its floating ice tongue, including surface depressions and basal crevasses creating full thickness rifts and tabular icebergs; D) Hektoria Glacier as it begins to calve at its grounding line (April 2022); E) Dynamic thinning of the lower glacier, with the ice plain nearing hydrostatic equilibrium and calving blocks buoyantly rotating, causing glacier earthquakes when capsizing against the terminus (November-December 2022); F) Hektoria Glacier retreats to a new more stable terminus position at the slope break or bedrock high (March 2023) and continues to calve, speed up, and dynamically thin.

Our results suggest that the differing grounding lines and evidence of clearly grounded ice behavior in the downstream glacier can be explained by the presence of an ice plain (Fig. 6), as first proposed by Tuckett et al.[28]. The two key differences between the geometries of Fig. 6 panels A and B are: 1) the landward limit of tidal flexure extends far beyond the grounding line and high tidal variations can change the location of true landward limit of tidal flexure Point F and may induce partial ungrounding of the glacier during high tides[21]; and 2) the ice plain area of the glacier is near hydrostatic equilibrium and is therefore sensitive to external perturbations[21] (e.g., fast ice break-up events). We conclude that this downstream Hektoria Glacier ice plain geometry facilitated the record-setting tidewater retreat when it thinned to near-flotation after the fast ice break-out in 2022.

Glacier response following the fast ice break-out

When the fast ice broke out in January 2022, the terminus of the ice tongue lost a small amount of buttressing[13,41] that mostly served to suppress calving[31]. This loss instigated an increase in rifting and the rapid disaggregation of the ice tongue into tabular icebergs. Unlike the Larsen B Ice Shelf collapse in 2002, optical imagery does not show substantial meltwater ponding that would have prompted rapid hydrofracture of the ice tongue rifts. Although an atmospheric river may have aided in the loss of the ice tongue[1,14], this occurred 7 months earlier and cannot explain the grounded ice retreat. When the rapid retreat initiated in early November 2022 there was no indication of melt ponding or warm weather events. However, warm conditions and incipient melt ponding on the adjacent Seal Nunataks Ice Shelf later in November 2022 may indicate some augmentation of calving events at Hektoria around that time. The most rapid retreat in December 2022 did not coincide with either warm weather or melt ponding, suggesting hydrofracture was an unlikely factor in the accelerated retreat (phase 3). Basal melting is unlikely to have affected conditions, as the Larsen B embayment has a cold oceanic water column[14].

Hektoria Glacier's accelerated retreat (phase 3), 8.2 ± 0.2 km in two months, is unprecedented in the modern glaciological record. Pfeffer[42] defines "rapid" as retreat rates that are greater than 200 m/yr, using Columbia Glacier, Alaska, as an example due to its 1000 m/yr retreat rate between 1980-2005 (refs.[42,43]). In Greenland, rapid retreats of several hundred meters per year are observed[44], including recently the 'Steenstrup' glacier retreat[45]. In Antarctica, Röhss Glacier on the James Ross Island lost 9.1 km of grounded ice, 7.5 km from January 2001-December 2001 (ref. [4]). The Röhss Glacier retreat occurred six years after the loss of the Prince Gustav Ice Shelf and continued until 2009, losing 70% of its area and retreating a total of 15 km (ref. [4]). This is not unlike a previous retreat of Hektoria itself 9 years after the loss of the Larsen B ice shelf, in which the glacier retreated 500 m from 10 February to 26 February in 2011 at a rate of at least 35 m/day (ref. [14]). Pope Glacier in West Antarctica experienced a grounding line retreat of 3.5 km in just four months[46], with bedrock profiles also indicative of ice plain geometry.

Hektoria Glacier's dynamical thinning is also globally unprecedented in the published record, at 80 ± 2 m/yr, measured over 6 months. This is higher than the thinning rates reported in Fluegel and Walker[14], likely due to a different measurement period. Earlier, HG was reported to have thinned ~38 m between March and September 2002 (ref. [11]). During this same period, Crane Glacier, south of HG, thinned over 100 m in ~two years, with ~40 m of thinning due to subglacial lake drainage[11,47]. Other fast-paced thinning rates occurred at HPS12 glacier, Patagonia and 'Steenstrup' Glacier, Greenland, at ~44 m/yr (ref. [48]) and ~50 m/yr (ref. [45]), respectively. Hektoria's exceptional thinning rate coincides with a ~6-fold increase in velocity, accelerating from 300 ± 40 m/yr to 1700 ± 40 m/yr by June 2023 (Fig. 3C).

Broader implications

Glacier instabilities, such as MICI and MISI, represent some of the greatest uncertainties in the future projection of sea level rise[49]. MICI is proposed to occur in various scenarios, dependent on cliff height (>100 m), the ice thickness gradient upstream, the water depth, and the amount of backstress from ice mélange at the glacier front[23,24]. At Hektoria, ice cliff heights rarely exceeded 60 m (ref. [14]; Fig. 3A, Extended Data Fig. 3) suggesting the theorized MICI was not a driver of the rapid retreat. Nor was the instability at Hektoria related to the classic MISI that requires a retreat into a retrograde bed slope.

Instead, our results show the rapid Hektoria retreat was induced by buoyancy-driven calving upon retreat into an ice plain and is perhaps representative of other grounding line instabilities[27,50], which can generate GEQ activity[27]. Using submarine glacial landforms, Graham et al.[50] propose that an ice plain geometry at Thwaites Glacier led to grounding line retreat at many meters per day within the last two centuries. Using similar methods, Batchelor et al.[27] inferred a rapid buoyancy-driven retreat of the Fennoscandian ice streams and ice shelves ~15-19 kya during the last glacial maximum. They infer retreat rates of 55-610 m/day, similar to Hektoria retreat rates in 2022 (Fig. 2). Hektoria's retreat may therefore represent a modern example of the rapid retreat process described by Batchelor et al.[27], albeit with rapid calving as a result of the grounding line retreat.

Ice plains have been detected in other areas of Antarctica, including Whillans Ice Stream[51], Bungenstockrücken[36], Institute Ice Stream[21,27], Pine Island Glacier[52], Ross Ice Shelf[53], Amery Ice Shelf[54], and Thwaites Glacier[27]. The loss of supporting ice shelves can in some cases instigate rapid thinning, bringing the ice plain to near hydrostatic equilibrium and initiating a rapid buoyancy-driven retreat, as observed in this study. Therefore, it is imperative to document the bedrock geometry beneath the glaciers around Antarctica to evaluate the potential for this type of instability to occur and incorporate rapid buoyancy-driven retreat in models predicting the fate of the Antarctic ice sheet.

Methods

Satellite image time-series for morphological evolution

We used MODIS (Moderate-Resolution Spectroradiometer), PlanetScope, Landsat 8 and 9, Worldview (WV) -1, 2, and 3, Sentinel-2, and Synthetic Aperture Radar (SAR; Sentinel-1) to investigate changes in glacier extent, characteristics, and dynamics. All these sensors were used to assess glacier surface and calving morphology, to infer crevassing and rifting styles, and to time the stages of retreat. The MODIS sensor, on the Aqua and Terra satellites, has a nearcontinuous daily image data archive from 2002 to present with coarse resolution (250-1000m). The Landsat 8 and 9 Operational Land Imager product has a panchromatic band with 15 m resolution and an orbital repeat time every 8-16 days. To assess smaller periods of rapid retreat, we used Sentinel-2 imagery acquired every 12 days (with 10 m resolution) and PlanetScope data, acquired by numerous small multispectral imaging satellites (1-5 m resolution). Additionally, we use WV-1, 2, and 3 satellite images that provide very high resolution (< 0.5 m) stereo-optical and multi-spectral images. Retreats were calculated by measuring the distance of the terminus from two separate images. We measured the retreat along the arch of the terminus every 100 m (approximately 9 data points) and averaged the distances. We used the standard error of the mean for the uncertainty.

Image-derived elevation and velocity changes

Satellite optical imagery was used for investigating the morphology and freeboard of icebergs and the creation of digital elevation models (DEMs) of the glacier surfaces. To evaluate elevation changes of surface features on Hektoria Glacier through the 2011-2022 period we utilized DEMs derived from ASTER (AST_L1A) data and SPOT5 HRS (1A) stereo-imagery. The DEM processing follows Bernat et al[56]. All the DEMs are co-registered and vertically adjusted to the 25 November 2006 SPOT5 DEM. This SPOT5 reference DEM is referred to the EGM96 geoid and was vertically coregistered to ICESat laser altimetry measurements from 2003 to 2009. The ASTER and other SPOT5 DEMs are vertically adjusted using low-elevation-change regions, such as bedrock outcrops. A single constant vertical offset is applied to each DEM. This results in a vertical uncertainty of about 5 m for ASTER DEMs and about 2 m for SPOT5 DEMs[57].

WV-1, 2, and 3 in-track stereo-image DEMs were obtained from the Polar Geospatial Center (PGC) to evaluate elevation changes post fast ice break-out. The DEMs have a spatial resolution of 2 m and absolute accuracy of ~±4 m in horizontal and vertical dimensions (from PGC documentation). We applied a geoid correction using EGM 2008 and then assessed the mean elevation difference (i.e., bias) for six bedrock regions in each of the WV DEMs relative to the Reference Elevation Map of Antarctica DEM (REMA)[58] and applied the mean offset to the WV DEMs, as done in Ochwat et al.[1]. The commonly known BedMachine[59] and Huss and Farinotti[60] bed maps differ dramatically for this area of the AP[61] and are inconsistent with the ice thicknesses we derived from iceberg freeboard and geometry.

Ice thickness and volume loss estimation

We calculated a minimum ice thickness for Hektoria Glacier using iceberg dimensions. We analyzed three high resolution satellite images during the time period of rapid retreat and measured the largest 9-10 rotated icebergs near the terminus of the glacier (Extended Data Fig. 1). We measured the length and width of the icebergs along the primary axes three times and averaged the three measurements. Here, ‘width’ refers to the longest dimension of the iceberg (assumed to be parallel to the surface when possible); ‘length’ refers to the maximum dimension perpendicular to the width axis. The largest length is the minimum ice thickness. To estimate the volume loss, we used the average minimum ice thickness from the three time periods of interest multiplied by the area loss. The area loss was determined by finding the mean of three measured area differences between two images. The reported uncertainties are the standard errors of the mean, propagated when necessary.

Ice flow speeds

To determine ice flow speeds through time we used standard feature tracking methods between consecutive pairs of Sentinel-1A and B SAR satellite images. From 2015 to 2017, Sentinel-1A provided 12-day image pairs and from 2017 until late 2021 and the addition of Sentinel-1B provided 6-day image pairs. We used the standard Gamma software to track coherent speckle and surface features between the image pairs. Surface structure must remain relatively constant in the pair interval, which is generally the case for the minimum repeat pairs[62]. We applied feature tracking to all image pairs of the 6 (when available) and 12-day repeat-pass period images for 2021-2023 and mosaiced all velocity maps into monthly averaged composites to give improved spatial consistency. Uncertainty in measured velocities depend on various factors including the delay between images (12 days or better), the pixels size (~10m), the error in satellite orbital parameters (negligible), the quality of features tracked between images (variable) and the number of image pairs contributing to each monthly mean (>=1). In general, however, the dominant factor is the precision achievable by the cross-correlation algorithm which, conservatively, is around one tenth of a pixel. In the worst case (12-day repeat, one image pair in a month), this leads to an uncertainty better than one tenth of 10m over 12 days, or ~ 0.1m/day (~40 m/year). Once the velocity mosaics were generated, we extracted ice speed profiles along the central flowline of Hektoria and Green Glacier. We also use the Inter-mission Land Ice Velocity Experiment (ITS_LIVE) velocity data to track the flow speed from 2011-2022 of four points along the central flow line of Hektoria Glacier using the ITS_LIVE mapping tool, with the days between image pairs ranging from 30-120 (ref.[55]).

Laser Altimetry

To study changes in surface ice elevation, we combined the WV image-derived DEMs with altimetry data from the Ice, Cloud, and Land Elevation Satellite 2 (ICESat-2), launched in 2018. We used the ICESat-2 ATL06 version 5 product, which provides a linear surface approximation of 40 m long overlapping segments along each ground track[63] with a 91-day repeat cycle (clouds permitting). We correct for the geoid (EGM 2008) prior to estimating the initial thickness of the fast ice, glacier tongues, and elevation of the glaciers. We use the along-track ICESat-2 data to examine thickness changes from 2018 to 2023. We extracted the WV DEM elevation data from 2017 to 2023 along the same track (RGT 1329 and 239) to fill in temporal gaps of the ICESat-2 data. To calculate the uncertainty of the thinning rate, we use the standard error of the mean. We averaged elevation data along the profile between -64.8410 and -64.8390° for both ICEsat-2 and Worldview DEMs and calculated the standard error of the mean of each date of data acquisition, then we propagated that error throughout all the dates.

Airborne radar profiles

Despite several attempts to map the base of the ice in the glacier fjords and ice tongue areas of the Larsen B embayment, a careful examination of the available IceBridge CReSIS radar data provides only very limited and subjective indications of the ice base in the central Hektoria Glacier outflow. From 2009 to 2018 IceBridge collected radar data in the HG region, however, most of the radar data near the Hektoria Glacier grounding zone have no reliable information on the bed signal and, hence, cannot be used for the glacier thickness and bed signal analysis. Nevertheless, the radar profile from 2017 shows a small area of the region with distinct reflections near the grounding zone. Here we followed the method in Antropova et al.[64] to assess the Normalized Bed Reflection Power (NBRP) and the Normalized Internal Reflection Power (NIRP) for the 2017 track 005. NBRP and NIRP indicate the power of the radar signal reflected from the bed of the glacier and within the ice column, respectively. NIRP serves as a qualitative assessment of the signal power losses. Hence, in general, we consider the NBRP signal reliable if it is higher than NIRP. Relatively high values of NBRP coefficients suggest the existence of water underlying the ice (i.e., floating ice), while low NBRP values indicate rocks and/or sediments under the ice layer[65,66]. We used the NBRP and NIRP to identify a transition zone between grounded and floating ice, limited by the available data (Extended Data Fig. 2), and compared it against the grounding line by Ochwat et al.[1].

Glacial-Earthquake Event-Detection, Location, and Waveform Modeling

Using the EarthScope Consortium seismic archive, including the POLENET Network, Antarctic Seismographic Argentinian-Italian Network, and the Global Seismograph Network, glacier earthquake (GEQ) detections were made using a grid search method that is broadly similar to previous studies[40]. We first downloaded and applied a bandpass filter (40-20s) the vertical component seismic data in the West Antarctic and Antarctic Peninsula region. We then computed envelopes using a 60 s short-term average to 1000 s long-term average (STA/LTA) ratio for each station. We selected time-windows with potential GEQs by finding 500 s time windows during which at least 3 stations have a peak STA/LTA ratio that exceeds 2.5. Next, we generated potential event sources on a 100 km grid that spanned the Antarctic continent. For each potential source, we shifted the envelopes to account for the expected travel time difference between the grid point and each station. The coherence of the shifted envelopes was then used as a measure of event location likelihood at the grid point. Since we were focused on finding potential glacial events in the Antarctic Peninsula region, we removed events with optimum locations outside the study region, defined by a bounding box that spanned -3000 to -1500 km (Polar Stereographic X) and from 500 to 2000 km (Polar Stereographic Y). For 2022, this resulted in approximately 40 event detections. Most of these events are tectonic earthquakes originating from the Southern Ocean that were incorrectly located due to the relatively small aperture of our network. We culled these events via visual inspection as the dispersive nature makes them very easy to distinguish from GEQs. We used GEQs to associate the calving with the grounded state of Hektoria Glacier.

To constrain event size and azimuth, we model the GEQs as a centroid single force (CSF)[39,67]. We download Green's functions from EarthScope Consortium's Syngine[68]. Due to the relatively low signal-to-noise ratios on the horizontal components of the seismograms, we were not able to estimate the dip of the source and prescribe it to be horizontal. We performed a simple grid search to obtain the optimal force and azimuth of the CSF that best reproduced the observed seismograms. As noted in previous work, there is a 180° ambiguity in the estimated azimuth that arises from the potential misalignment of the waveforms[67].

References

1. Ochwat, N. E., Scambos, T. A., Banwell, A. F., Anderson, R. S., Maclennan, M. L., Picard, G., Shates, J. A., Marinsek, S., Margonari, L., Truffer, M., Pettit, E. C. Triggers of the 2022 Larsen B multi-year landfast sea ice breakout and initial glacier response. The Cryosphere 18, 1709–1731 (2024).

2. Fürst, J. J., Durand, G., Gillet-Chaulet, F., Tavard, L., Rankl, M., Braun, M., Gagliardini, O. The safety band of Antarctic ice shelves. Nature Clim. Change 6, 479–482 (2016).

3. Gilbert, E., Kittel, C. Surface melt and runoff on Antarctic ice shelves at 1.5 °C, 2 °C, and 4 °C of future warming. Geophys. Res. Lett. 48, e2020GL091733 (2021).

4. Glasser, N. F., Scambos, T. A., Bohlander, J., Truffer, M., Pettit, E., Davies, B. J. From ice-shelf tributary to tidewater glacier: continued rapid recession, acceleration and thinning of Röhss Glacier following the 1995 collapse of the Prince Gustav Ice Shelf, Antarctic Peninsula. J. Glaciol. 57, 397–406 (2011).

5. Rott, H., Skvarca, P., Nagler, T. Rapid collapse of northern Larsen Ice Shelf, Antarctica. Science 271, 788–792 (1996).

6. Royston, S., Gudmundsson, G. H. Changes in ice-shelf buttressing following the collapse of Larsen A Ice Shelf, Antarctica, and the resulting impact on tributaries. J. Glaciol. 62, 905–911 (2016).

7. Rignot, E., Casassa, G., Gogineni, P., Krabill, W., Rivera, A., Thomas, R. Accelerated ice discharge from the Antarctic Peninsula following the collapse of Larsen B ice shelf. Geophys. Res. Lett. 31, 2004GL020697 (2004).

8. Scambos, T., Berthier, E., Haran, T., Shuman, C., Cook, A., Ligtenberg, S., Bohlander, J. Detailed ice loss pattern in the northern Antarctic Peninsula: widespread decline driven by ice front retreats. The Cryosphere 8, 2135–2145 (2014).

9. Rankl, M., Fürst, J. J., Humbert, A., Braun, M. H. Dynamic changes on the Wilkins Ice Shelf during the 2006–2009 retreat derived from satellite observations. The Cryosphere 11, 1199–1211 (2017).

10. Hulbe, C. L., Scambos, T. A., Youngberg, T., Lamb, A. K. Patterns of glacier response to disintegration of the Larsen B ice shelf, Antarctic Peninsula. Global Planet. Change 63, 1–8 (2008).

11. Scambos, T. A., Bohlander, J. A., Shuman, C. A., Skvarca, P. Glacier acceleration and thinning after ice shelf collapse in the Larsen B embayment, Antarctica. Geophys. Res. Lett. 31, 2004GL020670 (2004).

12. Needell, C., Holschuh, N. Evaluating the Retreat, Arrest, and Regrowth of Crane Glacier Against Marine Ice Cliff Process Models. Geophys. Res. Lett. 50, e2022GL102400 (2023).

13. Surawy-Stepney, T., Hogg, A. E., Cornford, S. L., Wallis, B. J., Davison, B. J., Selley, H. L., Slater, R. A., Lie, E. K., Jakob, L., Ridout, A. L. The impact of landfast sea ice buttressing on ice dynamic speedup in the Larsen-B Embayment, Antarctica. The Cryosphere 2023, 1–24 (2024).

14. Fluegel, B. L., Walker, C. The two-decade evolution of Antarctica's Hektoria Glacier and its 2022 rapid retreat from satellite observations. Geophys. Res. Lett. 51, e2024GL110592 (2024).

15. Bassis, J. N., Walker, C. C. Upper and lower limits on the stability of calving glaciers from the yield strength envelope of ice. Proc. R. Soc. A. 468, 913–931 (2012).

16. Pollard, D., DeConto, R. M., Alley, R. B. Potential Antarctic Ice Sheet retreat driven by hydrofracturing and ice cliff failure. Earth Planet. Sci. Lett. 412, 112–121 (2015).

17. Parizek, B. R., Christianson, K., Alley, R. B., Voytenko, D., Vaňková, I., Dixon, T. H., Walker, R. T., Holland, D. M. Ice-cliff failure via retrogressive slumping. Geology 47, 449–452 (2019).

18. Schoof, C. Marine ice sheet stability. J. Fluid Mech. 698, 62–72 (2012).

19. Favier, L., Durand, G., Cornford, S. L., Gudmundsson, G. H., Gagliardini, O., Gillet-Chaulet, F., Zwinger, T., Payne, A. J., Le Brocq, A. M. Retreat of Pine Island Glacier controlled by marine ice-sheet instability. Nature Clim. Change 4, 117–121 (2014).

20. Gudmundsson, G. H., Paolo, F. S., Adusumilli, S., Fricker, H. A. Instantaneous Antarctic ice sheet mass loss driven by thinning ice shelves. Geophys. Res. Lett. 46, 13903–13909 (2019).

21. Brunt, K. M., Fricker, H. A., Padman, L. Analysis of ice plains of the Filchner–Ronne Ice Shelf, Antarctica, using ICESat laser altimetry. J. Glaciol. 57, 965–975 (2011).

22. Friedl, P., Weiser, F., Fluhrer, A., Braun, M. H. Remote sensing of glacier and ice sheet grounding lines: A review. Earth Sci. Rev. 201, 102948 (2020).

23. Crawford, A. J., Benn, D. I., Todd, J., Åström, J. A., Bassis, J. N., Zwinger, T. Marine ice-cliff instability modeling shows mixed-mode ice-cliff failure and yields calving rate parameterization. Nat. Commun. 12, 2701 (2021).

24. Bassis, J. N., Berg, B., Crawford, A. J., Benn, D. I. Transition to marine ice cliff instability controlled by ice thickness gradients and velocity. Science 372, 1342–1344 (2021).

25. Melton, S. M., Alley, R. B., Anandakrishnan, S., Parizek, B. R., Shahin, M. G., Stearns, L. A., Finnegan, D. C. Meltwater drainage and iceberg calving observed in high-spatiotemporal resolution at Helheim Glacier, Greenland. J. Glaciol. 68, 812–828 (2022).

26. Murray, T., Selmes, N., James, T. D., Edwards, S., Martin, I., O'Farrell, T., Aspey, R., Rutt, I., Nettles, M., Baugé, T. Dynamics of glacier calving at the ungrounded margin of Helheim Glacier, southeast Greenland: Dynamics of glacier calving. J. Geophys. Res. Earth Surf. 120, 964–982 (2015).

27. Batchelor, C. L., Christie, F. D. W., Ottesen, D., Montelli, A., Evans, J., Dowdeswell, E. K., Bjarnadóttir, L. R., Dowdeswell, J. A. Rapid, buoyancy-driven ice-sheet retreat of hundreds of metres per day. Nature 617, 105–110 (2023)

28. Tuckett, P. A., Ely, J. C., Sole, A. J., Livingstone, S. J., Davison, B. J., van Wessem, J. M. Reply to: "Impact of marine processes on flow dynamics of northern Antarctic Peninsula outlet glaciers" by Rott et al. Nature Commun. 11, 2970 (2020).

29. Alley, R. B., Cuffey, K. M., Bassis, J. N., Alley, K. E., Wang, S., Parizek, B. R., Anandakrishnan, S., Christianson, K., DeConto, R. M. Iceberg calving: regimes and transitions. Annu. Rev. Earth Planet. Sci. 51, 189–215 (2023).

30. Sulak, D. J., Sutherland, D. A., Enderlin, E. M., Stearns, L. A., Hamilton, G. S. Iceberg properties and distributions in three Greenlandic fjords using satellite imagery. Ann. Glaciol. 58, 92–106 (2017).

31. Robel, A. A. Thinning sea ice weakens buttressing force of iceberg mélange and promotes calving. Nat. Commun. 8, 14596 (2017).

32. Rott, H., Abdel Jaber, W., Wuite, J., Scheiblauer, S., Floricioiu, D., van Wessem, J. M., Nagler, T., Miranda, N., van den Broeke, M. R. Changing pattern of ice flow and mass balance for glaciers discharging into the Larsen A and B embayments, Antarctic Peninsula, 2011 to 2016. The Cryosphere 12, 1273–1291 (2018).

33. Wallis, B. J., Hogg, A. E., Zhu, Y., Hooper, A. Change in grounding line location on the Antarctic Peninsula measured using a tidal motion offset correlation method. The Cryosphere, 18, 4723–4742 (2024)

34. Anandakrishnan, S., Voigt, D., Alley, R., & King, M. Ice stream D flow speed is strongly modulated by the tide beneath the Ross Ice Shelf. Geophysical Research Letters 30 (2003)

35. Voytenko, D., Stern, A., Holland, D. M., Dixon, T. H., Christianson, K., & Walker, R. T. Tidally driven ice speed variation at Helheim Glacier, Greenland, observed with terrestrial radar interferometry. Journal of Glaciology 61, 301–308 (2015)

36. Freer, B. I., Marsh, O. J., Hogg, A. E., Fricker, H. A., Padman, L. Modes of Antarctic tidal grounding line migration revealed by ICESat-2 laser altimetry. The Cryosphere 1–35 (2023).

37. Sergeant, A., Mangeney, A., Yastrebov, V. A., Walter, F., Montagner, J.-P., Castelnau, O., Stutzmann, E., Bonnet, P., Ralaiarisoa, V. J.-L., Bevan, S. Monitoring Greenland ice sheet buoyancy-driven calving discharge using glacial earthquakes. Ann. Glaciol. 60, 75–95 (2019).

38. Olsen, K. G., Nettles, M., Cathles, L. M., Burton, J. C., Murray, T., James, T. D. Improved estimation of glacial-earthquake size through new modeling of the seismic source. J. Geophys. Res. Earth Surf. 126, e2021JF006384 (2021).

39. Nettles, M., Ekström, G. Glacial earthquakes in Greenland and Antarctica. Annu. Rev. Earth Planet. Sci. 38, 467–491 (2010).

40. Winberry, J. P., Huerta, A. D., Anandakrishnan, S., Aster, R. C., Nyblade, A. A., Wiens, D. A. Glacial earthquakes and precursory seismicity associated with Thwaites Glacier calving. Geophys. Res. Lett. 47, e2019GL086178 (2020).

41. Parsons, R., Sun, S., Gudmundsson, G. H., Wuite, J., Nagler, T. Quantifying the buttressing contribution of landfast sea ice and mélange to Crane Glacier, Antarctic Peninsula. The Cryosphere 18, 5789–5801 (2024)

42. Pfeffer, W. T. A simple mechanism for irreversible tidewater glacier retreat. J. Geophys. Res. 112, 2006JF000590 (2007).

43. O'Neel, S., Pfeffer, W. T., Krimmel, R., Meier, M. Evolving force balance at Columbia Glacier, Alaska, during its rapid retreat. J. Geophys. Res. 110, 2005JF000292 (2005).

44. Catania, G. A., Stearns, L. A., Sutherland, D. A., Fried, M. J., Bartholomaus, T. C., Morlighem, M., Shroyer, E., Nash, J. Geometric controls on tidewater glacier retreat in central western Greenland. JGR Earth Surf. 123, 2024–2038 (2018).

45. Chudley, T.R., Howat, I.M., King, M.D. and Negrete, A., Atlantic water intrusion triggers rapid retreat and regime change at previously stable Greenland glacier. Nature Communications, 14(1), 2151, (2023).

46. Milillo, P., Rignot, E., Rizzoli, P., Scheuchl, B., Mouginot, J., Bueso-Bello, J. L., ... & Dini, L. Rapid glacier retreat rates observed in West Antarctica. Nature Geoscience, 15, 48–53. (2022).

47. Shuman, C. A., Berthier, E., Scambos, T. A. 2001–2009 elevation and mass losses in the Larsen A and B embayments, Antarctic Peninsula. J. Glaciol. 57, 737–754 (2011).

48. Dussaillant, I., Berthier, E., Brun, F., Masiokas, M., Hugonnet, R., Favier, V., Rabatel, A., Pitte, P., Ruiz, L. Two decades of glacier mass loss along the Andes. Nature Geosci. 12, 802–808 (2019).

49. Fox-Kemper, B., et al. in Climate Change 2021: The Physical Science Basis. Contribution of Working Group I to the Sixth Assessment Report of the Intergovernmental Panel on Climate Change (eds. Masson-Delmotte, V., et al.) 1211–1362 (IPCC, Cambridge Univ. Press, 2021). (2021)

50. Graham, A. G. C., Wåhlin, A., Hogan, K. A., et al. Rapid retreat of Thwaites Glacier in the pre-satellite era. Nat. Geosci. 15, 706–713 (2022).

51. Bindschadler, R., Vornberger, P., Gray, L. Changes in the ice plain of Whillans Ice Stream, West Antarctica. J. Glaciol. 51, 620–636 (2005).

52. Corr, H. F., Doake, C., Jenkins, A., Vaughan, D. G. Investigations of an "ice plain" in the mouth of Pine Island Glacier, Antarctica. J. Glaciol. 47, 51–57 (2001).

53. Freer, B. I. D., Marsh, O. J., Fricker, H. A., Hogg, A. E., Siegfried, M. R., Floricioiu, D., et al. Coincident lake drainage and grounding line retreat at Engelhardt Subglacial Lake, West Antarctica. J. Geophys. Res. Earth Surf. 129, e2024JF007724 (2024).

54. Fricker, H. A., Coleman, R., Padman, L., Scambos, T. A., Bohlander, J., Brunt, K. M. Mapping the grounding zone of the Amery Ice Shelf, East Antarctica using InSAR, MODIS, and ICESat. Antarctic Sci. 21, 515–532 (2009).

55. Gardner, A., Fahnestock, M., Scambos, T. MEaSUREs ITS_LIVE Landsat image-pair glacier and ice sheet surface velocities. Version 1 (2019).

Acknowledgements

We would like to thank NASA for funding our research and our fieldwork in 2024. We thank CIRES for continued support, particularly CIRES travel and Dawn Williams. We thank the Instituto Antártico Argentino for supporting our fieldwork to the Antarctic Peninsula and the helicopter pilots who flew us over Hektoria Glacier. We thank the many conversations with Doug Benn, Anna Crawford, Tasha Snow, Catherine Walker, Ben Wallis, Sierra Melton, and countless others. EB and MB acknowledge support from the French Space Agency (CNES).

Funding: Include all funding sources, including grant numbers, complete funding agency names, and recipient's initials. Each funding source should be listed in a separate paragraph such as:

National Aeronautics and Space Administration Grant: 80NSSC22K0386

Author contributions:

Conceptualization: NEO, TAS, RSA
Methodology: NEO, TAS, AL, EB, MB, JPW, YKA
Data Curation: NEO, AL, EB, MB, JPW, YKA
Investigation: NEO
Visualization: NEO, YKA
Supervision: TAS, RSA
Writing—original draft: NEO
Writing—review & editing: NEO, TAS, RSA, AL, EB, MB, JPW, MB, YKA

Competing interests: All other authors declare they have no competing interests.

Data and materials availability: IceBridge radar data is publicly available on the CReSIS webpage https://data.cresis.ku.edu/. All Landsat-8 and 9, MODIS, and ICESat-2 data are publicly available on https://search.earthdata.nasa.gov/. Sentinel-1 and 2 data were provided by the Copernicus Program of the European Union and are publicly available on https://browser.dataspace.copernicus.eu/. Planet and Worldview data are available in the main text Fig.s and supplementary materials. Sentinel-1 velocities are available in the main text. ASTER and SPOT5 HRS imagery are freely available respectively at https://search.earthdata.nasa.gov/ and https://regards.cnes.fr/user/swh/, corresponding DEMs are available upon request. All seismic data were downloaded from the EarthScope Consortium Web Services including data from the POLENET Network (10.7914/SN/YT_2007), Antarctic Seismographic Argentinean Italian Network (10.7914/SN/AI), and the Global Seismograph Network (10.7914/SN/IU).

Methods References

56. Bernat, M., Belart, J., Berthier, E., Jóhannesson, T., Hugonnet, R., Dehecq, A., Magnússon, E., Gunnarsson, A. Geodetic mass balance of Mýrdalsjökull Ice Cap, 1999–2021. Jökull 73, 35–53 (2023).

57. Berthier, E., Scambos, T. A., Shuman, C. A. Mass loss of Larsen B tributary glaciers (Antarctic Peninsula) unabated since 2002. Geophys. Res. Lett. 39 (2012).

58. Howat, I. M., Porter, C., Smith, B. E., Noh, M.-J., Morin, P. The reference elevation model of Antarctica. The Cryosphere 13, 665–674 (2019).

59. Morlighem, M., Rignot, E., Binder, T., Blankenship, D., Drews, R., Eagles, G., Eisen, O., Ferraccioli, F., Forsberg, R., Fretwell, P., Goel, V., Greenbaum, J. S., Gudmundsson, H., Guo, J., Helm, V., Hofstede, C., Howat, I., Humbert, A., Jokat, W., Karlsson, N. B., Lee, W. S., Matsuoka, K., Millan, R., Mouginot, J., Paden, J., Pattyn, F., Roberts, J., Rosier, S., Ruppel, H., Seroussi, H., Smith, E. C., Steinhage, D., Sun, B., van den Broeke, M. R., van Ommen, T. D., van Wessem, M., Young, D. A. Deep glacial troughs and stabilizing ridges unveiled beneath the margins of the Antarctic ice sheet. Nature Geosci. 13, 132–137 (2020).

60. Huss, M., Farinotti, D. A high-resolution bedrock map for the Antarctic Peninsula. The Cryosphere 8, 1261–1273 (2014).

61. Shahateet, K., Navarro, F., Seehaus, T., Fürst, J. J., Braun, M. Estimating ice discharge of the Antarctic Peninsula using different ice-thickness datasets. Ann. Glaciol. 64(91), 121–132 (2023).

62. Luckman, A., Quincey, D., Bevan, S. The potential of satellite radar interferometry and feature tracking for monitoring flow rates of Himalayan glaciers. Remote Sens. Environ. 111, 172–181, (2007).

63. Smith, B., Fricker, H. A., Holschuh, N., Gardner, A. S., Adusumilli, S., Brunt, K. M., ... & Siegfried, M. R. Land ice height-retrieval algorithm for NASA's ICESat-2 photon-counting laser altimeter. Remote Sensing of Environment 233, 111352, (2019).

64. Antropova, Y. K., Mueller, D., Samsonov, S. V., Komarov, A. S., Bonneau, J., & Crawford, A. J. Grounding-line retreat of Milne Glacier, Ellesmere Island, Canada over 1966–2023 from satellite, airborne, and ground radar data. Remote Sensing of Environment 315, 114478, (2024).

65. Gades, A. M., Raymond, C. F., Conway, H., & Jagobel, R. Bed properties of Siple Dome and adjacent ice streams, West Antarctica, inferred from radio-echo sounding measurements. Journal of Glaciology 46, 88–94, (2000).

66. Copland, L. & Sharp, M. Mapping thermal and hydrological conditions beneath a polythermal glacier with radio-echo sounding. Journal of Glaciology 47, 232–242 (2001).

67. Walter, F., Amundson, J. M., O'Neel, S., Truffer, M., Fahnestock, M., & Fricker, H. A. Analysis of low-frequency seismic signals generated during a multiple-iceberg calving event at Jakobshavn Isbræ, Greenland. Journal of Geophysical Research: Earth Surface 117, (2012).

68. Krischer, L., Hutko, A. R., van Driel, M., Stähler, S., Bahavar, M., Trabant, C., & Nissen-Meyer, T. On-demand custom broadband synthetic seismograms. Seismological Research Letters 88, 1127–1140, (2017).

Extended Data for

Record grounded glacier retreat caused by an ice plain calving process in Antarctica

N. Ochwat et al.

*Corresponding author. Email: naomi.ochwat@colorado.edu

Extended Data Fig. 1.

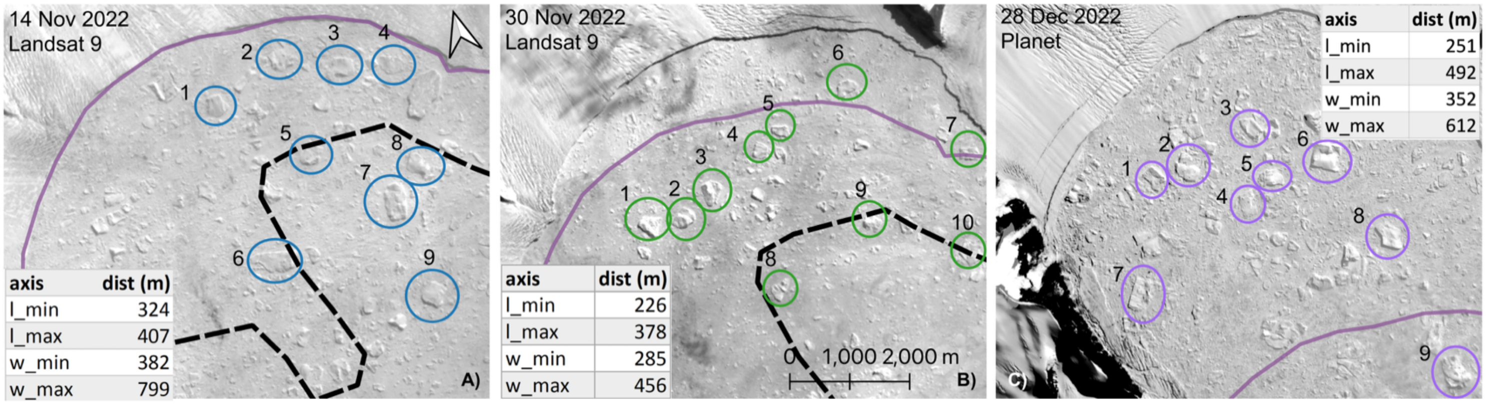

Iceberg distribution size during three calving events used to estimate ice thickness. The black dashed line is the grounding zone from our earlier study[1] and the purple line is the ice front on 14 November 2022. The three panels share the same scale and depict different areal extents. Here, ‘width’ refers to the longest dimension of the iceberg; ‘length’ refers to the maximum dimension perpendicular to the width axis. The largest length is the minimum ice thickness. A) Average of nine icebergs resulted in an minimum ice thickness of 407 ± 11 m. B) Average of ten icebergs resulted in a minimum ice thickness of 378 ± 18 m. C) Average of nine icebergs resulting in a minimum ice thickness of 492 ± 30 m.

Extended Data Fig. 2.

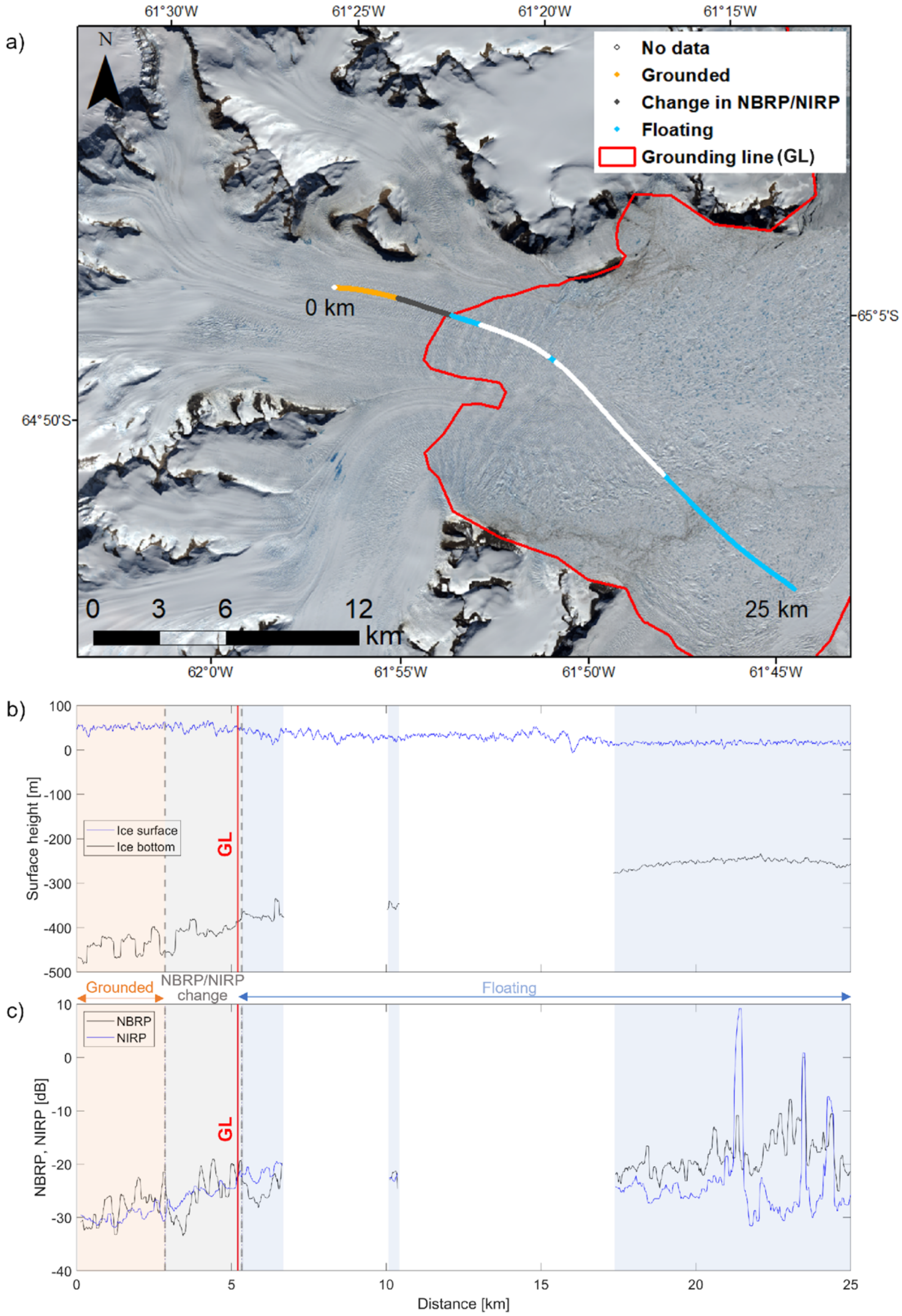

IceBridge dataset acquired over Hektoria Glacier on 31 October 2017 A) IceBridge track overlying a true-color Landsat-8 optical image acquired on 3 December 2017. The red contour and line is Ochwat et al.[1] grounding line. B) Ice surface and bottom heights; C) Normalized Bed Reflection Power (NBRP) and Normalized Internal Reflection Power (NIRP). The grounded part of the glacier associated with relatively low NBRP values is highlighted by light orange color, the floating ice associated with relatively high NBRP values is highlighted by blue color, and the region where both NBRP and NIRP values start to increase is highlighted by gray color. This region is likely associated with the transition of the glacier from grounded to floating, however, the bed signal at the beginning of this zone is obscured by high internal reflection (NIRP > NBRP) associated with the crevasses clearly seen in the Landsat-8 images (Panel A).

Extended Data Fig. 3

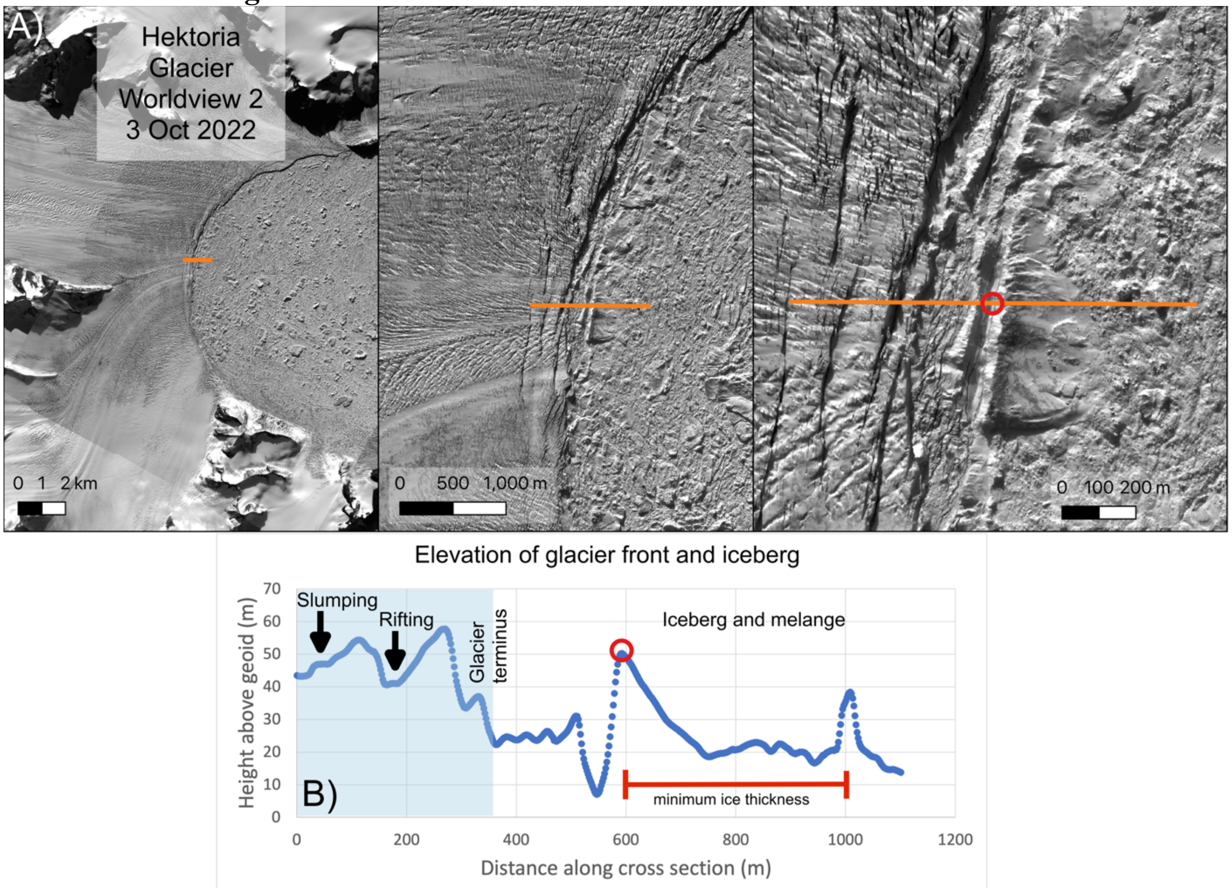

Terminus of Hektoria Glacier at the grounding line. A) series of Worldview 2 orthoimage on 3 October 2022 at different zoomed levels. B) Elevation profile at glacier front from Worldview derived DEM on 3 October 2022. The terminus has a ~50 m high cliff front and displays slumping and rifting upstream of the terminus. The iceberg at the front is clearly rotated “bottom-out” indicating it was calved via buoyancy-driven processes.

Extended Data Fig. 4

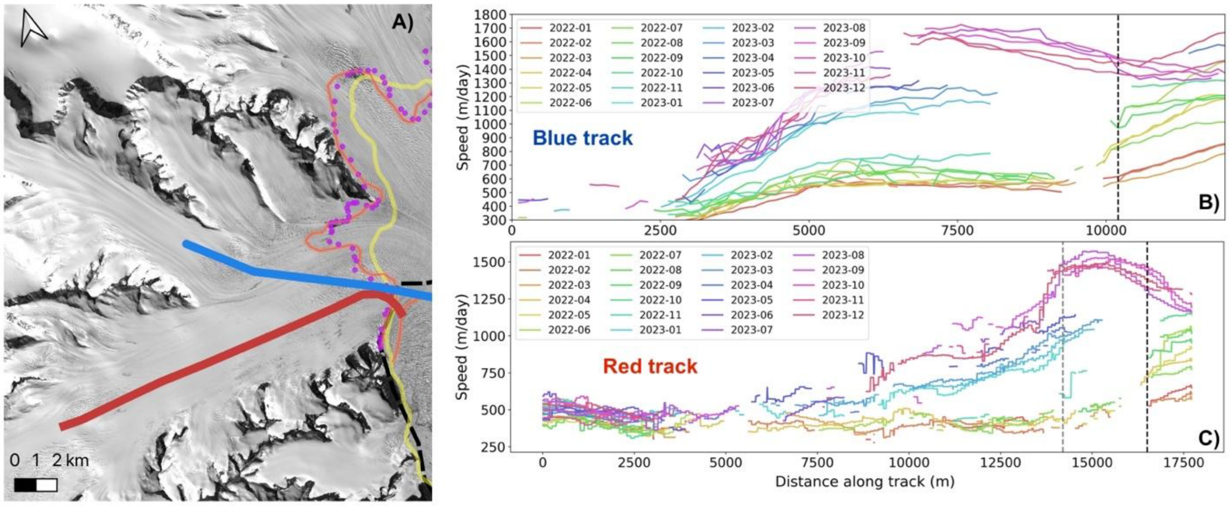

Green Glacier velocity from January 2022 to December 2023. A) tracks where velocity was extracted. Depicts the along-flow profile (red line, panel B) and the Icebridge ATM track profile (blue line, panel C) in order to compare the speeds to those presented in Ochwat et al.[1]. Ochwat et al.[1] show a speed increase in Green Glacier of 500 m/yr to 1150 m/yr by January 2023, and here we show the speed has continued to increase to 1700 m/yr by December 2023 (measured at 7500 m distance along track), representing ~3.5-fold increase in speed since the loss of the fast ice. At 11 km upstream of the Green Glacier terminus the glacier flow speed has yet to be affected by the loss of the fast ice and new calving regime. Green Glacier underwent similar phases of change as Hektoria, yet only retreated 4.5 km of grounded ice through austral winter 2023. Since then, Green Glacier has undergone several periods of minimal advancement and subsequent retreat of up to 2 km until April 2024 and is still actively calving and retreating.

Extended Data Fig. 5

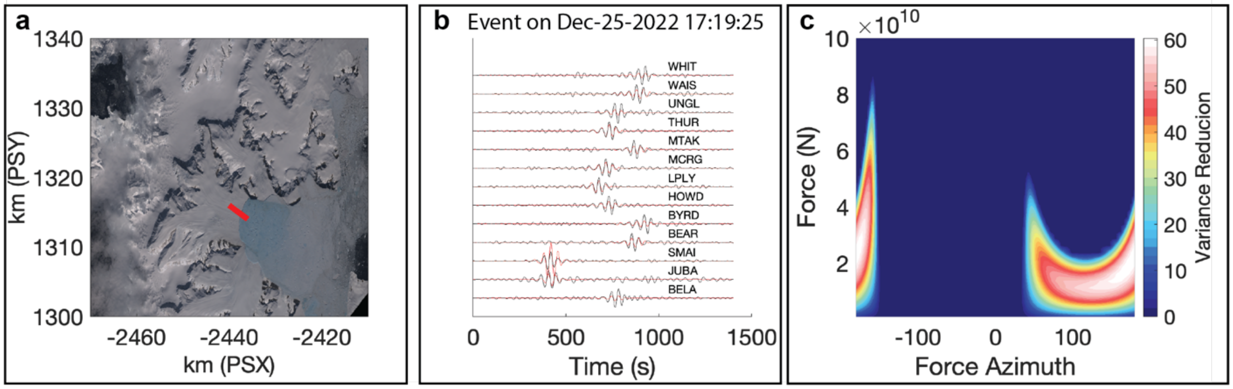

Example of waveform modeling for Dec 25, 2022 Event. A) Landsat image from December 8, 2022 with the force vector inferred from the modeling of the waveforms. Note: force vector has been placed manually near the calving front of Hektoria Glacier for visual clarity. B) the bandpass-filtered (20-50s) observed (black) and synthetic (red) waveforms from a grid search for horizontal force magnitude and direction. Stations are sorted by distance to location. C) variance reduction as a function force azimuth and magnitude.

Extended Data Table 1

Event Arrival Time @LPLY	Peak Force	Azimuth
Nov-6-2022 20:08:32	3.5×10^{9} N	164
Nov-6-2022 20:49:31	6.1×10^{9} N	-170
Dec-12-2022 06:02:58	2.1×10^{10} N	168
Dec-12-2022 13:15:14	8.6×10^{9} N	172
Dec-19-2022 05:59:45	1.37×10^{10} N	170
Dec-25-2022 17:19:25	1.9×10^{10} N	174

Event times and estimate force magnitudes and directions for the 6 observed GEQs that we observed to originate from the Hektoria Glacier region.

*We report event arrival time at station LPLY since it is the closest station to the source location(s) of the GEQs for which the seismic arrival is clearly observed for all events.

Supplemental Video 1:

Timelapse of Sentinel-1 SAR imagery from November 2021 to February 2025.

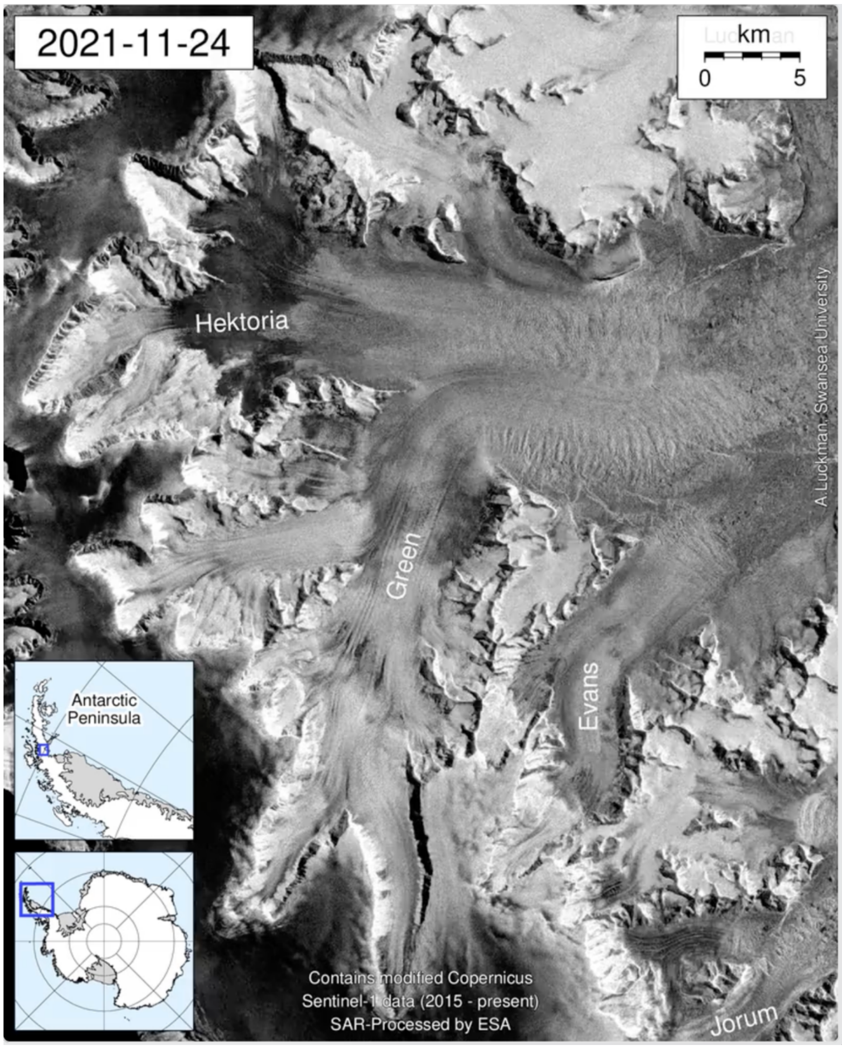

Supplemental Video 2

GoPro footage of Hektoria Glacier reconnaissance flight 26 February 2024 courtesy of Captain Franco Saravalli Fuerza Aérea Argentina.